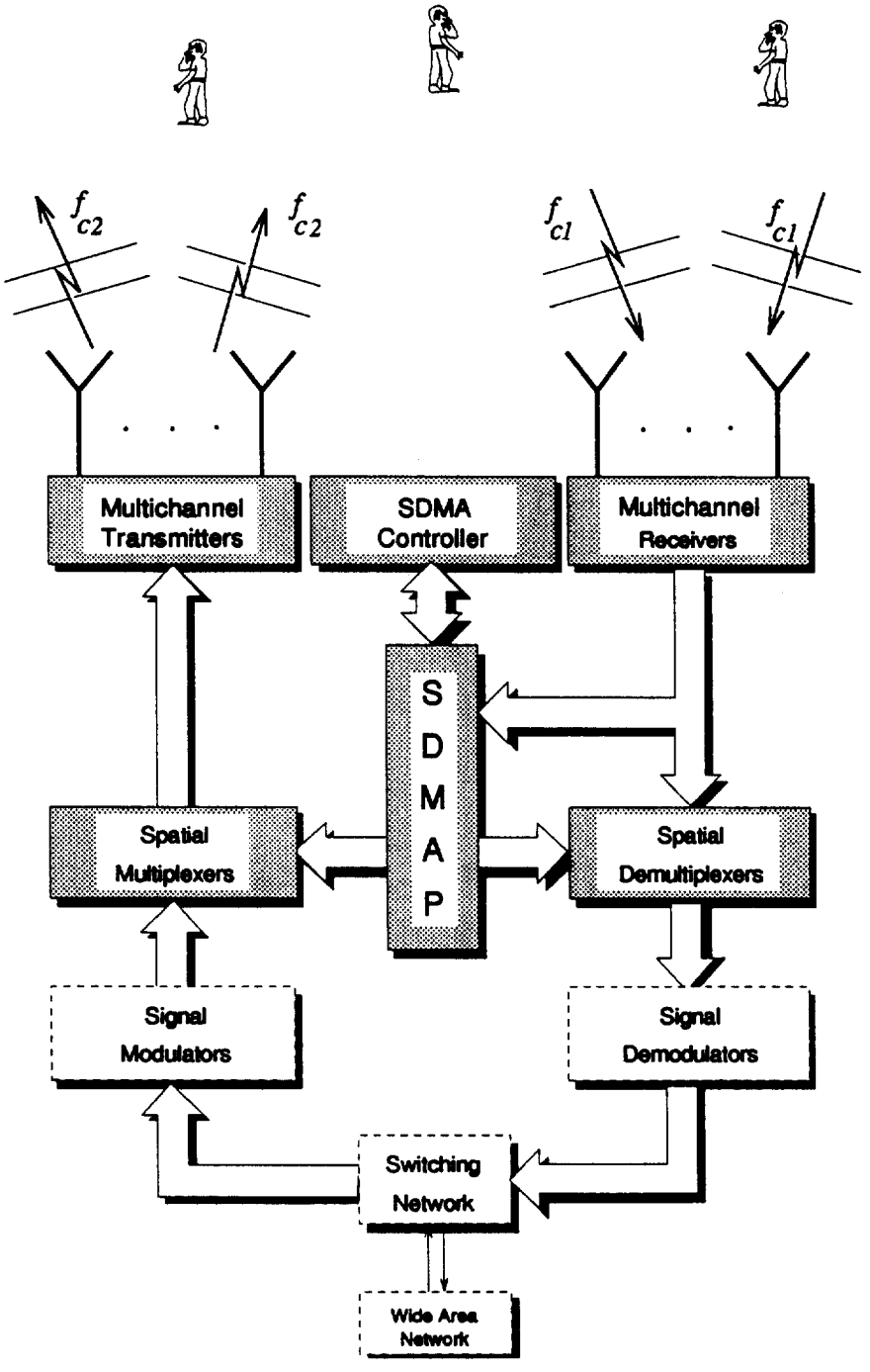

Figure 1-1: Block diagram of WCN employing SDMA

SDMA employs an array of antennas for reception and transmission[1]. Typically, the array will be composed of simple, identical, uniformly spaced, collinear antennas. Received signals pass through a reception and downconversion stage, at which point they are available to the SDMA processor (SDMAP) and the spatial demultiplexers. Within the SDMAP, the antenna data is processed to determine the the number of users present on the channel and to generate the information necessary to demultiplex the co-channel signals. Using this information the spatial demultiplexer separates the users' signals, after which the signals are demodulated (FM demodulation in the case of AMPS voice signals) and passed on to the existing wireline network. Complementary operations are performed on transmission. Information provided by the SDMAP allows the spatial multiplexer to combine signals on a single frequency channel so that each user receives their intended signal without interference from the other users' signals. In an actual AMPS application of SDMA, this processing scheme would be replicated for each frequency pair within a cell.

SDMA's impact on the hardware costs associated with a base station are quite modest. Continuing with our AMPS example, low power (*e.g.* 10W) amplifiers are inexpensive and readily available. The spatial multiplexers and demultiplexers could be implemented with low-cost digital signal processing chips. The processor at the heart of the SDMAP could be a conventional microprocessor like the Motorola 68040. A system very much like this was inexpensively constructed to support the investigations described in Section 4. Because the antenna array is composed of simple identical elements, it, too, has a low cost. Theoretically, the maximum number of co-channel users is equal to one less than the number of elements in the antenna array. A conservative design, accounting for equipment outages and multipath, would support half as many co-channel users as there are antennas in the array. Employing an array with elements spaced at half the nominal AMPS wavelength of 0.35m (880MHz), a ten element array, only 1.75m in length, would provide a factor of five capacity increase within each cell. Conversion of an existing AMPS system to an SDMA AMPS system can therefore be accomplished at a very modest incremental cost, providing, in the example above, a factor of five increase in capacity while retaining compatibility with existing user units (handsets). Similar calculations can be made for other types of WCN's.

Motivated by the substantial potential economic impact of SDMA technology, the Phase I effort concentrated on an exploration of some practical issues associated with its implementation and performance. The remainder of this report consists of four sections. The first section is an executive summary, which is followed by a description of experimental objectives and apparatus. Experimental results are then presented. The last section of the report provides conclusions and suggestions for future research directions.

[1]The same array can be used for transmission and reception. The arrays are depicted separately in the figure for illustrative purposes.

2. Executive Summary

This SBIR contract final report describes results obtained during the Phase I effort that demonstrated the feasibility of applying state of the art sensor array signal processing to the problems of increasing capacity and quality of current and future wireless communication systems. The original proposal outlined several theoretical problems that could be addressed. At the beginning of the contract period, however, the opportunity to construct brassboard experimental hardware presented itself. The project therefore took on a more practical approach, with two basic objectives: validation of the theoretical results in a practical setting, and the collection of experimental data for additional algorithm development and refinement.

During the course of this effort, experimental apparatus for the reception and transmission of multiple co-channel communication signals was constructed, and a variety of receive-only and transmit-only experiments were conducted. Data collected with this equipment was then processed off-line to assess system performance. This apparatus may be considered as initial hardware and software prototypes for some of the SDMA concepts outlined in the original proposal.

For reception, these preliminary experiments indicate that it is possible to resolve sources less than 0.4 Rayleigh beamwidths apart to within fractions of a degree and that closely spaced co-channel sources can be successfully demodulated. On transmission, more than 30dB of isolation was obtained for receivers spaced at 1.2 Rayleigh beamwidths, demonstrating the ability to effect separate spatial channels. The overall conclusion to be drawn from the Phase I effort is that SDMA technology has the potential of dramatically increasing both the capacity and quality of current and future wireless communication systems. These improvements are accomplished by use of state-of-the art signal processing algorithms and hardware in concert with multiple antennas.

The Phase II effort will be to build an operational full-duplex SDMA system that would simultaneously locate, track, and communicate with multiple mobile wireless units from a single base station. This prototype will be used to investigate the validity of RF environment models incorporated in the signal processing algorithms, to identify SDMA system issues requiring further investigation, and to evaluate robust candidate solutions thereto. Research into multitarget tracking, complex RF propagation, and adaptive real-time algorithms will also be conducted during this investigative phase.

3. Objectives and Apparatus

Our original Phase I proposal outlined a number of theoretical issues that might benefit from further investigation. These included some issues related to fast algorithms, tracking of multiple targets, and characterization of WCN radio environments. As stated earlier, the opportunity to construct experimental apparatus presented itself, and, as practical experimental investigations of the basic SDMA technology are clearly more valuable than simulations thereof, we decided to take the more practical approach. Preliminary assessments indicated that calculation speed was not an issue and that the algorithms could be easily implemented on off-the-shelf processors.

The basic objectives were to implement a sensor array for both reception and transmission, to validate the theoretical results in a practical setting, and to collect experimental data for additional algorithm development and refinement. Off-line analysis was performed on the data to verify that the technology could be made to work as part of a real-time system.

Three different sets of experiments were conducted. The first two sets tested receive-only and transmit-only performance with both pure tones and digital communications signals. These tests were conducted in an anechoic chamber to eliminate anomalous propagation effects such as multipath. Of course, the anechoic chamber also eliminates the background radio frequency (RF) energy present in a realistic communications environment. As compensation, a small amount of noise was added to the received signals in the anechoic chamber reception experiments. The third set of tests were transmit-only tests using frequency modulated music signals in a realistic environment (office building interior) that might be encountered in a personal communications system (PCS).

The prototype system constructed for the anechoic chamber experiments employed an array of of six vertical dipole elements (approximately 6cm in length or $\lambda/2$ at 2.5GHz) mounted 17cm from a ground plane as depicted in Figure 3-1. RF absorbing material was placed between the elements (which were themselves mounted on PVC pipe with epoxy) and the backplane to minimize reflections and the effects of resonance. The cost of materials for the array was on the order of $200. The SDMA Processor consisted of a digital signal processing (DSP) board controlled by a personal computer (PC). In turn, the DSP controlled a 12-channel digital-to-analog converter (DAC). The PC was used to collect calibration information on the apparatus, calculate the appropriate SDMA transmission or reception strategy, and then download the appropriate code to the DSP to establish the spatial communications channels (*i.e.* spatial (de)multiplexing). Single Sideband (SSB) transmission was employed, with the multichannel transmitters and receivers respectively requiring or providing both in-phase (I) and quadrature (Q) components of the modulated signal. The overall receiver/transmitter chain was calibrated to minimize carrier leakage and maximize image rejection by appropriately adjusting the I and Q amplitude biases and relative phase. Array calibration was achieved via a simple sequential technique for obtaining the array manifold information necessary for the SDMA processor. Relative locations of the array elements are shown in Figure 3-2.

The third set of tests, in the office building interior, used a similar experimental setup except that the array consisted of four commercial AMPS dipole antennas with radomes,

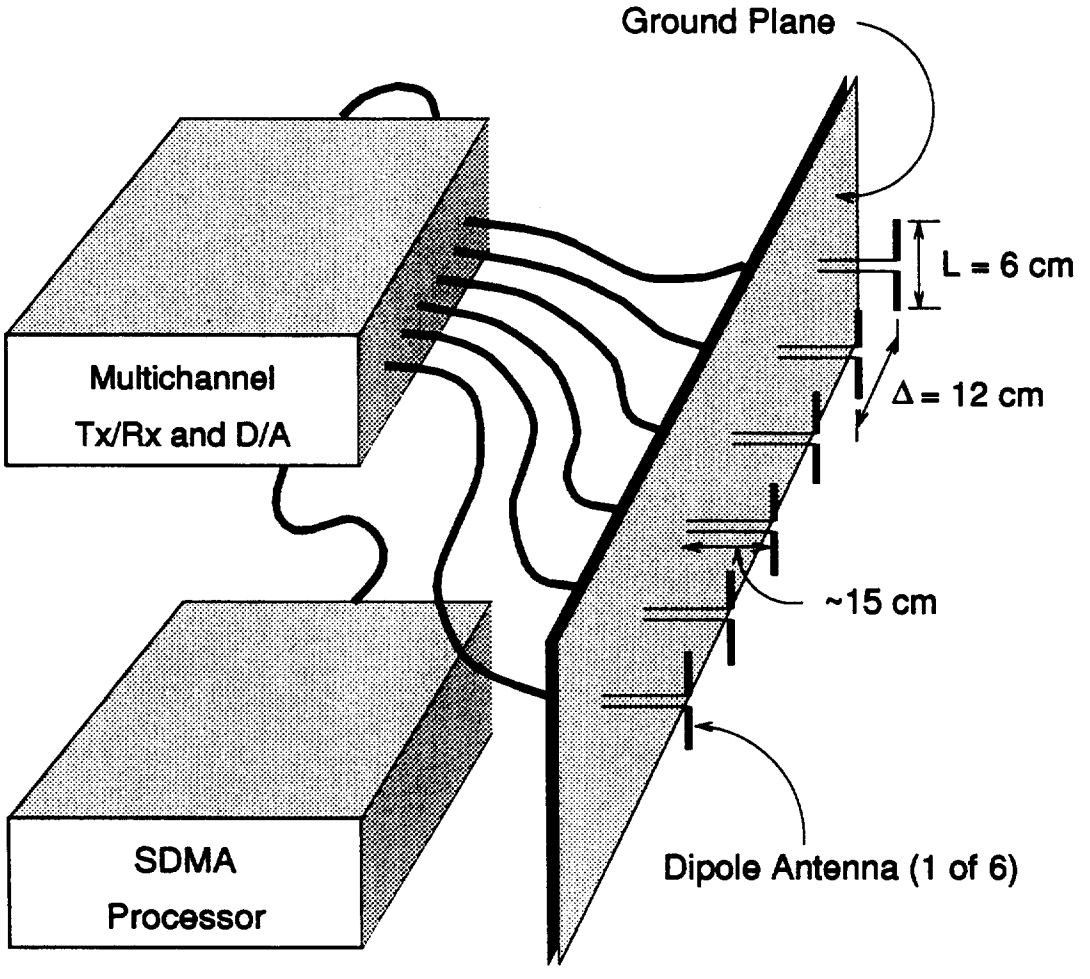

Figure 3-1: SDMA prototype system

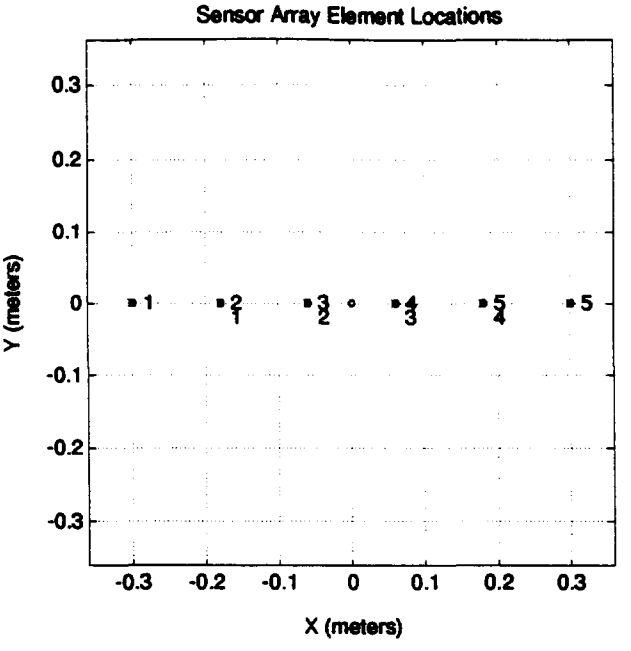

Figure 3-2: Experimental uniform linear array (ULA) element relative locations

uniformly spaced along a wood backing plate and with the axis of the array oriented horizontally. The elements were spaced 14in apart, which corresponds roughly to a one wavelength spacing for the 850MHz frequency at which the experiments were conducted.

4. Experimental Results

4.1 Anechoic Chamber Experiments: BFSK Reception

In the anechoic chamber reception experiments, a binary frequency-shift-keyed (BFSK) modulation scheme similar to that of second generation cordless phone (CT-2) systems was employed. The phrase *signal copy* appears in some of the plots, it has the same meaning as spatial demultiplexing. The acronym ULA refers to a uniform linear array such as the one employed in these experiments.

4.1.1 Two Sources Closely Spaced

Two vertically polarized sources were used in the first experiment. The center frequency (or RF carrier) was set to 1.200GHz resulting in half-wavelength ($\lambda/2$) adjacent element spacing. The baud rate was set to 2KHz for both waveforms. One signal used a 2KHz modulation deviation, a 5 KHz modulation deviation was used for the other. These baud rates and deviations were chosen so as to minimize any distortion effects

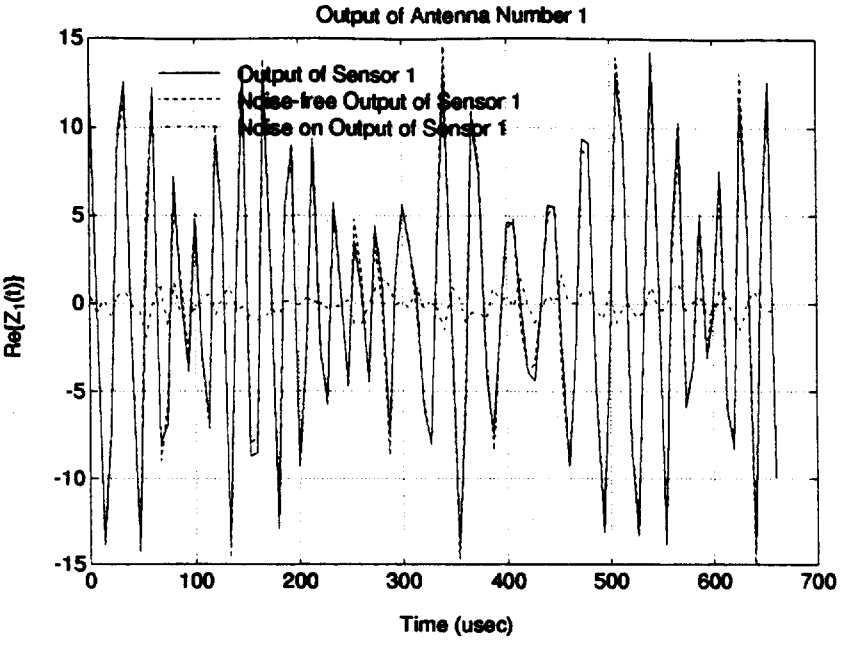

Figure 4-1: Experimental ULA output of sensor number 1 – Case 1

resulting from the front-end anti-aliasing and image rejection filters. The multichannel data were sampled at 150KHz, and up to 8192 samples were taken from each of the 6 antennas.

The signals were set at approximately 20dB and 14dB above the noise, resulting in respective carrier-to-interference (C/I) ratios of +6dB and -6dB, with azimuths of 100° and 110° with respect to the axis of the array. Figure 4-1 displays the (real part of the) output of sensor 1 along with the (real part of the complex) noise.

SDMA processing yielded the direction of arrival (DOA) estimates displayed in Table 4-1. The estimates are based upon 4096 snapshots. The results clearly manifest the

Parameter	Estimate	True Value
$\hat{\theta}_1$	100.5°	100°
$\hat{\theta}_2$	110.1°	110°

Table 4-1: DOA estimates for two closely spaced sources

ability of SDMA to localize two co-channel sources well within a Rayleigh beamwidth. Figure 4-2 displays the spatially demultiplexed signals along with the transmitted and residual (or difference) signals. Post-processing C/I ratios are approximately 30dB as evidenced by the residuals. The signals have successfully been spatially demultiplexed and are easily decoded.

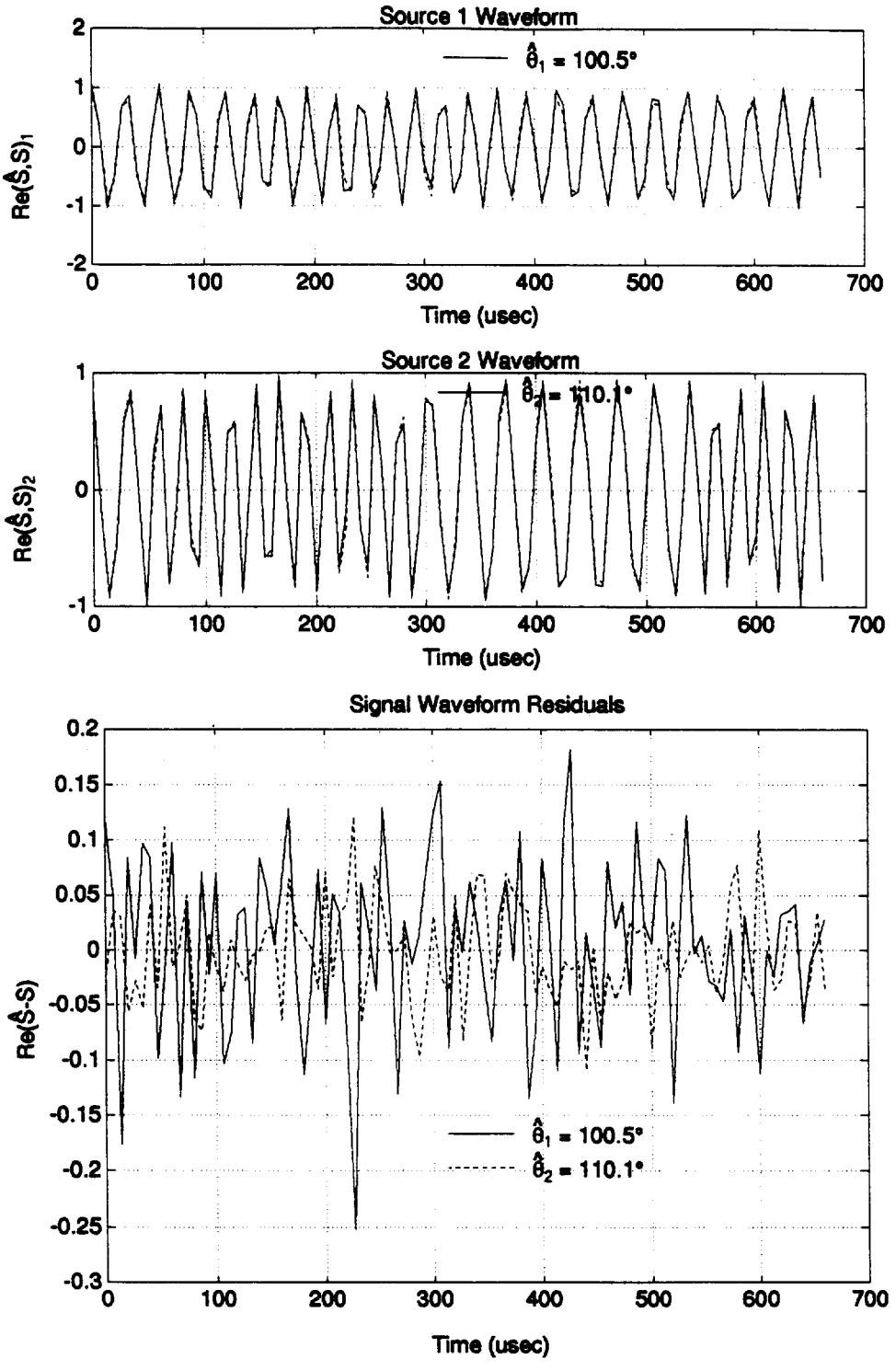

Figure 4-2: Experimental signal copy results – Case 1

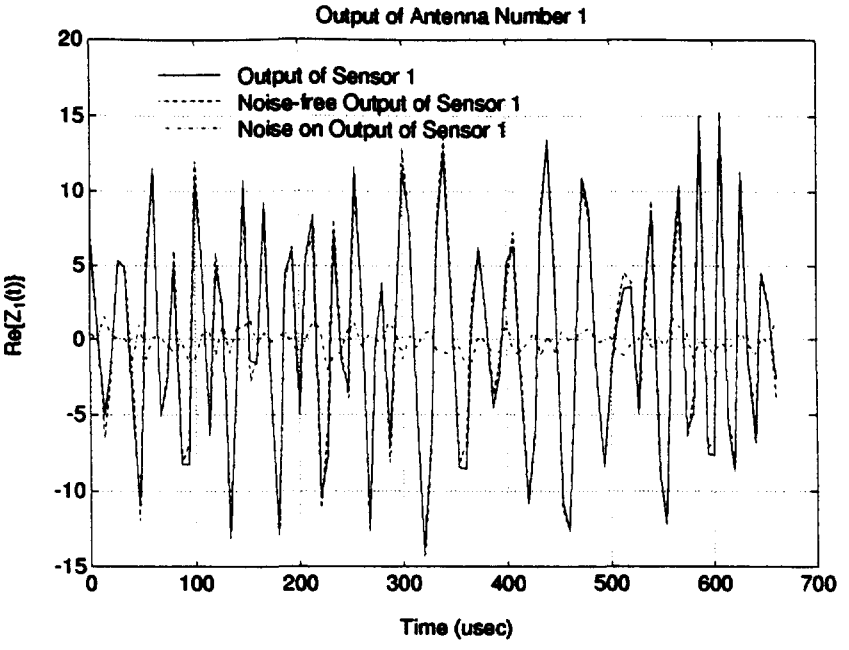

Figure 4-3: Experimental ULA output of sensor number 1 - Case 2

4.1.2 Two Source Case with Rayleigh Fading

To investigate the effects of Rayleigh-type fading on SDMA system performance, a third source was added, coherent with the first and placed 2° away. Thus, for this test there were two coherent sources at 68° and 70°, and a second independent source at 110°. The simulated multipath for the first (70°) source was attenuated by 3dB and delayed by a small fraction of a baud, thereby representing a nearby scattering center with a scattering coefficient magnitude of 0.5. The output of sensor 1 is shown in Figure 4-3 along with the (real part of the complex) noise.

As is typical of Rayleigh fading, the multipath cluster appears as a single source and the estimated direction-of-arrival indicates the location of the cluster. Estimated source DOA's for this case, based upon 4096 snapshots, are provided in Table 4-2. The

Parameter	Estimate	True Value
$\hat{\theta}_1$	80.3°	78°-80°
$\hat{\theta}_2$	110.1°	110°

Table 4-2: DOA estimates with multipath

results clearly demonstrate the ability of SDMA to localize two co-channel sources in the presence of this Rayleigh fading (near multipath). The spatially demultiplexed signals are displayed in Figure 4-4 along with the transmitted and residual signals. As indicated by the residuals in Figure 4-4, the post-processing C/I ratios are approximately 20–

30dB. Again, the signals have been successfully spatially demultiplexed and are easily demodulated and decoded.

4.1.3 Three Source Case

SDMA continues to provide accurate bearing estimates in the presence of three sources. Independent sources were located at 65°, 90°, and 110° with amplitudes 10, 5, and 10 relative to unit power noise respectively. The (real part of the) output of sensor 1 is shown in Figure 4-5 along with the (real part of the complex) noise. The estimated source DOA's, based upon 4096 snapshots, are displayed in Table 4-3.

Parameter	Estimate	True Value
$\hat{\theta}_1$	64.6°	65°
$\hat{\theta}_2$	90.1°	90°
$\hat{\theta}_3$	109.7°	110°

Table 4-3: DOA estimates with three independent sources

These results clearly indicate the ability of SDMA to localize three co-channel sources in close proximity with varying power levels. Figure 4-6 displays the spatially demultiplexed signal along with transmitted signal and residual signals. As indicated in the residuals in Figure 4-6, the post-processing C/I ratios are approximately 20–30dB. Compared to the initial C/I of approximately -6dB, this represents a processing gain of approximately 35dB.

4.2 Anechoic Chamber Experiments: Tone and BPSK Transmission

We now describe the anechoic chamber SDMA transmission tests. The experiments were conducted at a center frequency of 850MHz with transmitted power levels of approximately 10dBm through each of the six elements. The data was collected with a single channel receiver employing a two-stage down conversion with intermediate filtering for image rejection. The real (I) receiver channel was sampled at a 150KHz rate and digitized.

Experiments were conducted using both sinusoidal and binary phase-shift keyed (BPSK) waveforms. 10KHz and 20KHz sine waves were used in the tone tests; the BPSK waveforms were formed from repeated random bit sequences of length 2048 imposed on a 20KHz modulation of the 850MHz carrier. Up to two signals were transmitted, one to 270° (broadside) and the second to 225°. The 225° azimuth was intentionally selected to coincide with the peak of the first sidelobe in the 90° array gain pattern, presenting a maximal challenge. The separation of 45° corresponds to approximately 1.2 Rayleigh beamwidths.

The objective of these experiments was to demonstrate distinct spatial transmission channels with equal powers in the two preferred directions and a minimum of mutual

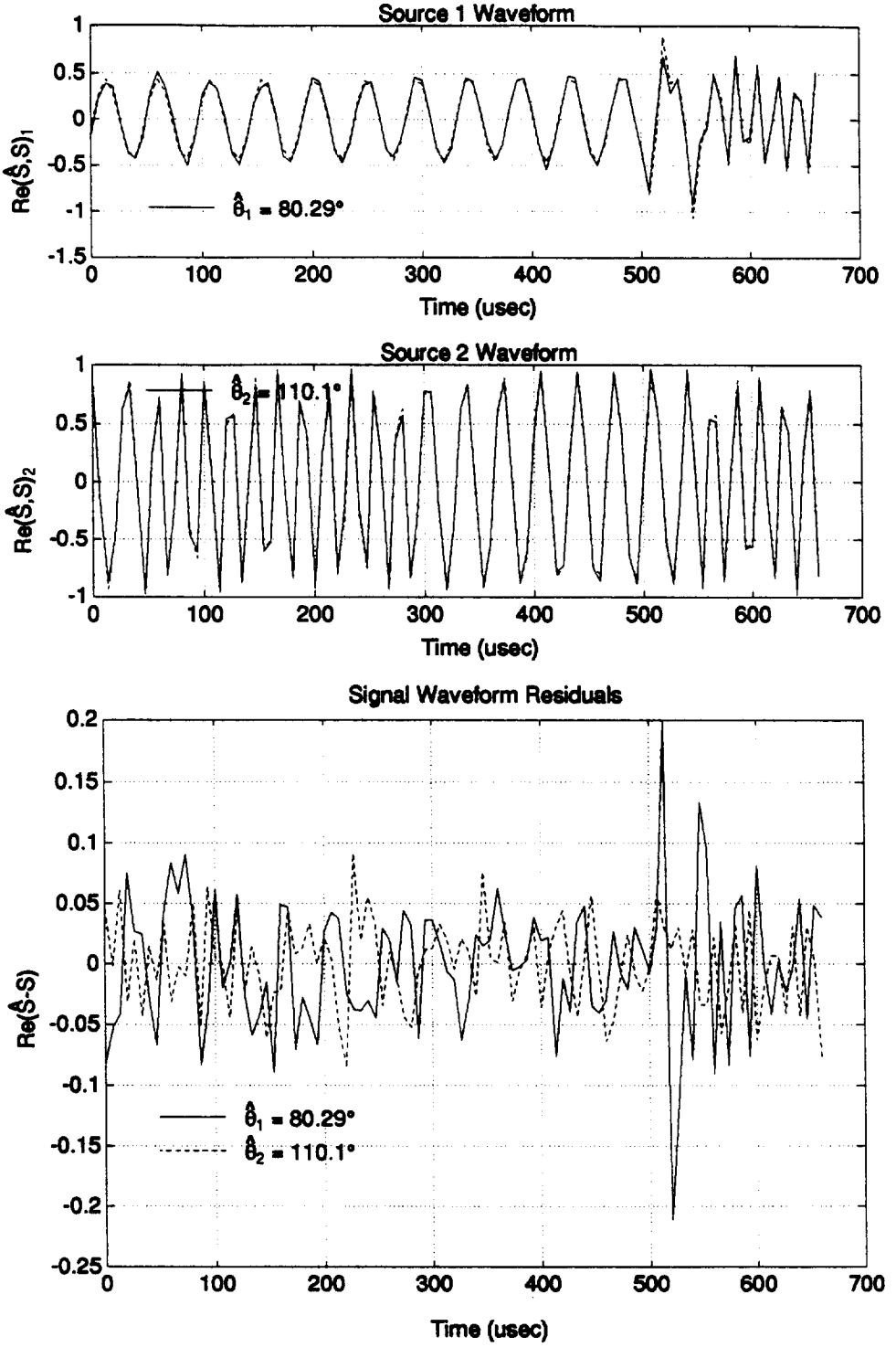

Figure 4-4: Experimental signal copy results – Case 2

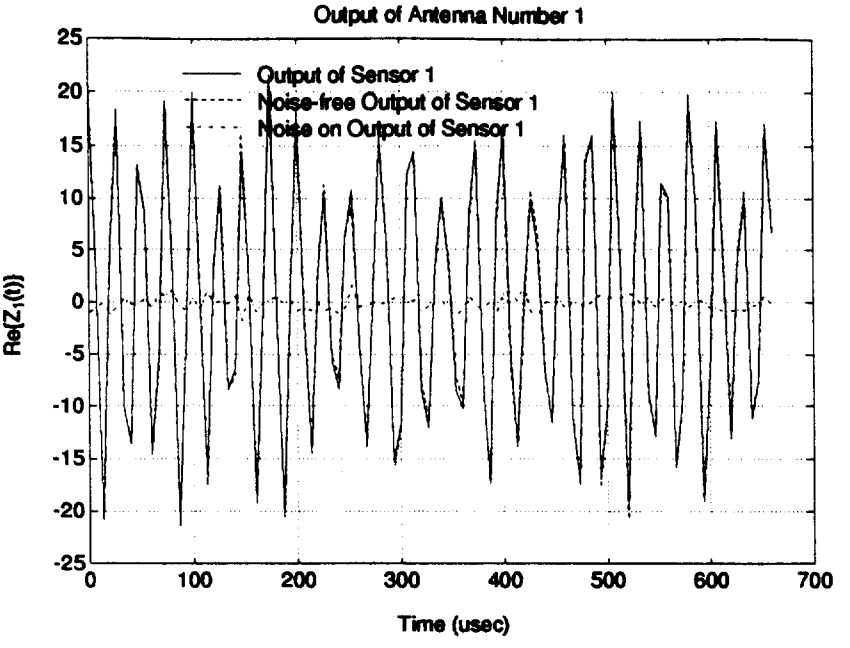

Figure 4-5: Experimental ULA output of sensor number 1 - Case 2

interference. Theoretical analyses predict for a six element array that a given power level at the receiver can be attained with approximately 1/6 the total transmitted power required if only a single antenna were employed. This prediction was validated by our experiments. Reductions in required transmitter power have a direct impact on the economics and quality of the services provided by WCN's: less expensive transmitters can be employed, battery lifetimes are extended in mobile units, and the level of background RF "pollution" experienced by other users within that portion of the spectrum is reduced.

4.2.1 Pure tones

The spatial distribution of RF energy for the sinusoidal transmission tests is given in Figures 4-7 through 4-9. Figure 4-7 displays the results of a a single 20KHz tone directed at 270°, with suppression at 225° desired. Due to imperfect absorption in the anechoic chamber wall containing the door to the chamber, and the fact that the main beam was directed at the walls when the array was oriented such that the 225° null was pointed toward the receiver, there was a substantial amount of scattering present in this case. This scattering accounts for the fact that only 20dB of rejection was observed around 225°. Still, this rejection was sufficient to allow essentially error-free demodulation of the BPSK waveform as detailed below.

Figure 4-8 corresponds to a single 20KHz tone was directed at 225°, with suppression at 270° desired. In this case the main beam was directed at the opposite wall of the chamber, a significant reduction in scattering was therefore observed. The experimental

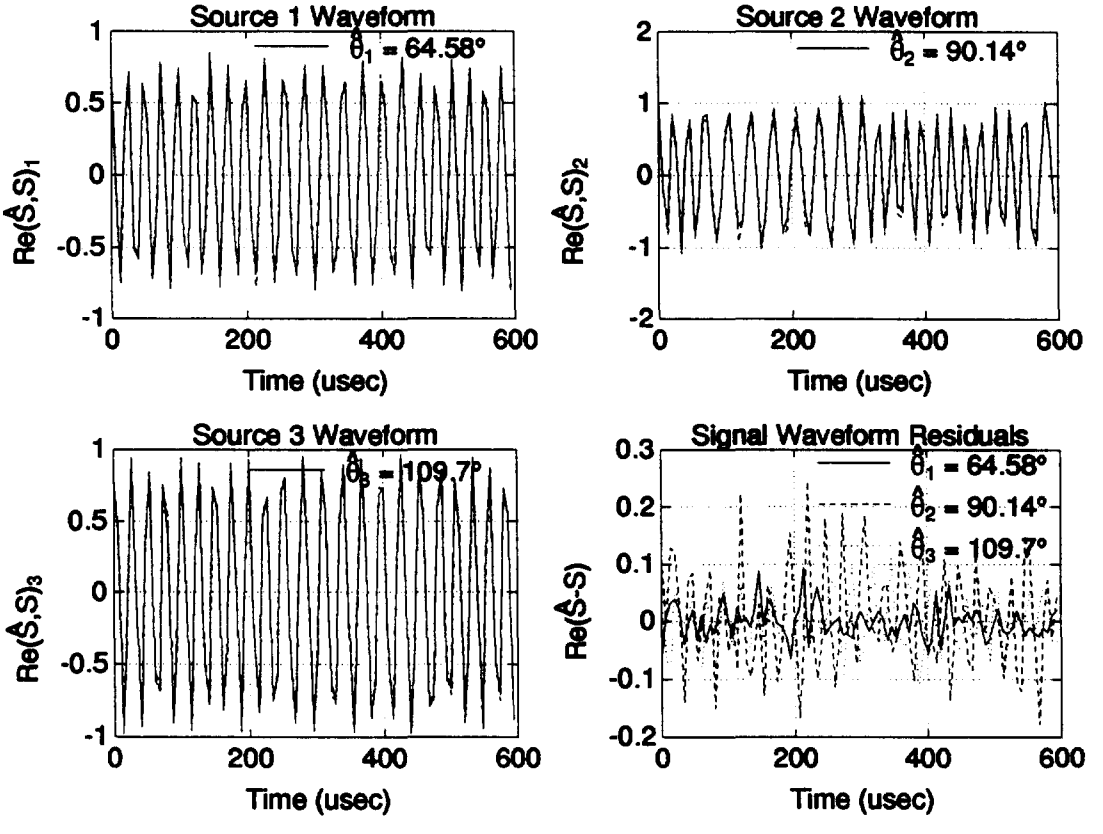

Figure 4-6: Experimental signal copy results – Case 3

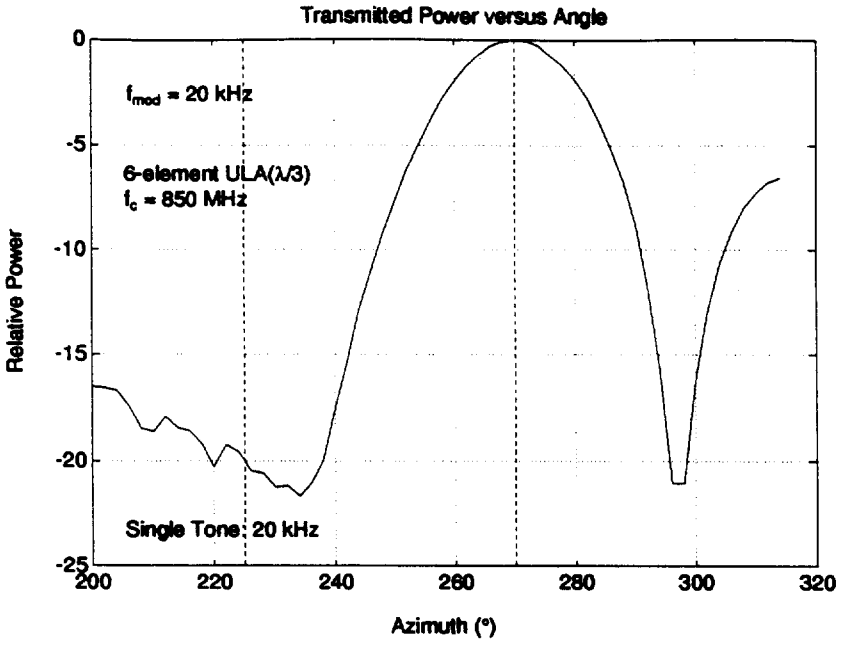

Figure 4-7: Measured spatial directivity for a single 20KHz tone directed to 270° with rejection at 225°

pattern is quite similar to that which would be obtained from an ideal uniform linear array with the same design objectives.

In Figure 4-9 we display the results of two tones transmitted simultaneously — the first a 20KHz tone directed at 270° with suppression at 225° desired, and the second a 10KHz tone directed at 225° with suppression at 270° desired. The figure contains plots of power at the appropriate modulation frequency as a function of azimuthal angle. The desired directivity was clearly achieved. Figure 4-10 is a contour plot of the same data showing array directivity as a function of both azimuth and frequency. (The ridges therein are the curves in the previous two figures.)

These experimental results clearly indicate that it is possible to simultaneously transmit two different signals on the same carrier to spatially distinct receivers with sufficient isolation to allow near perfect signal reconstruction. Examples of signal reconstruction are provided in the following section.

Note that in these experiments, the transmission weights for the array elements were computed using a simple deterministic model for the signals. This accounts for the deep nulls in the array's spatial directivity that can be observed in Figures 4-7 through 4-9. Although this strategy for computing transmissions weights worked well in the present context, in the real world the receivers' locations will not be known exactly. Transmission weight calculations that incorporate uncertainty concerning the receiver locations will be important in a practical implementation and will be therefore be investigated as part of the Phase II research.

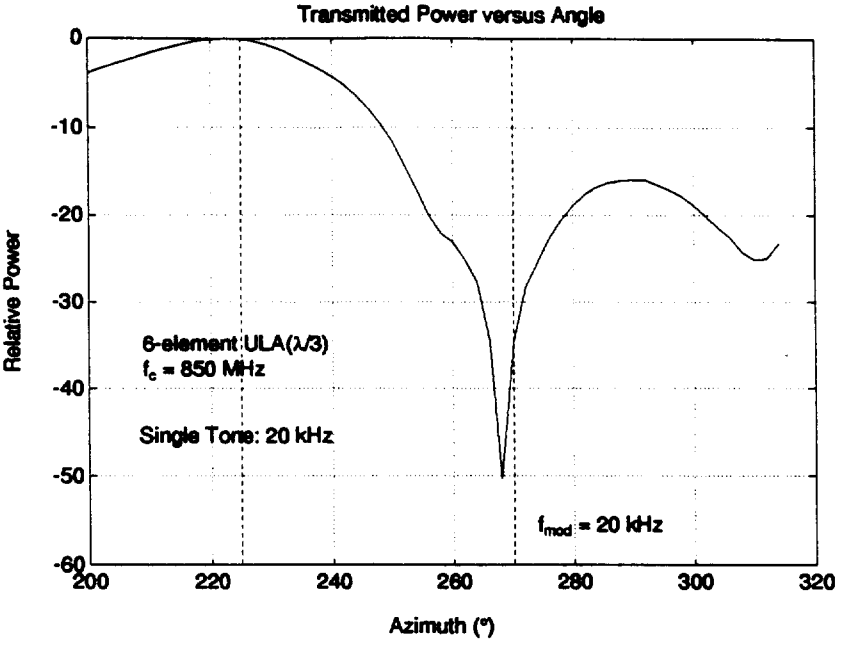

Figure 4-8: Measured spatial directivity for a single 20KHz tone directed to 225° with rejection at 270°

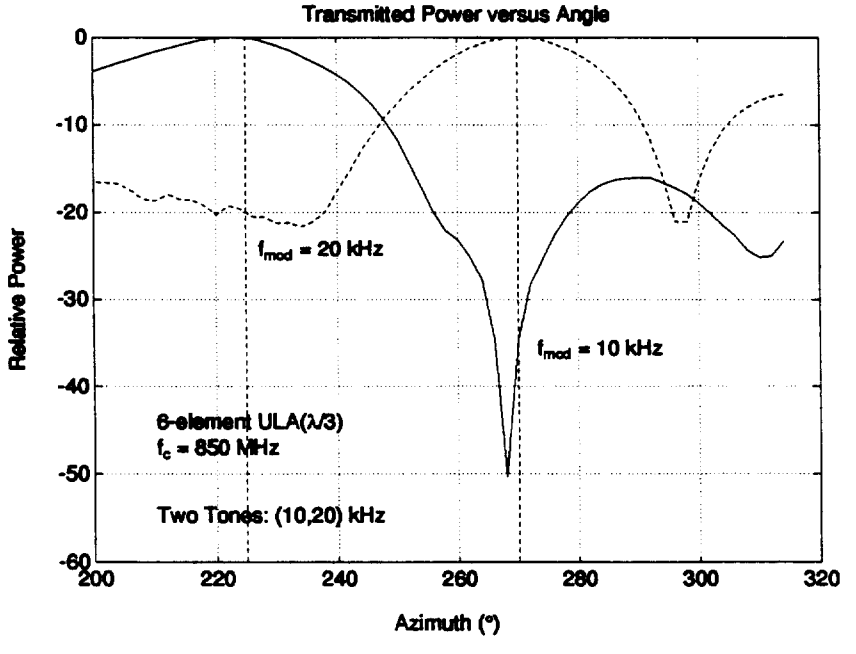

Figure 4-9: Measured spatial directivity for 10KHz and 20KHz tones directed to 225° and 270° respectively

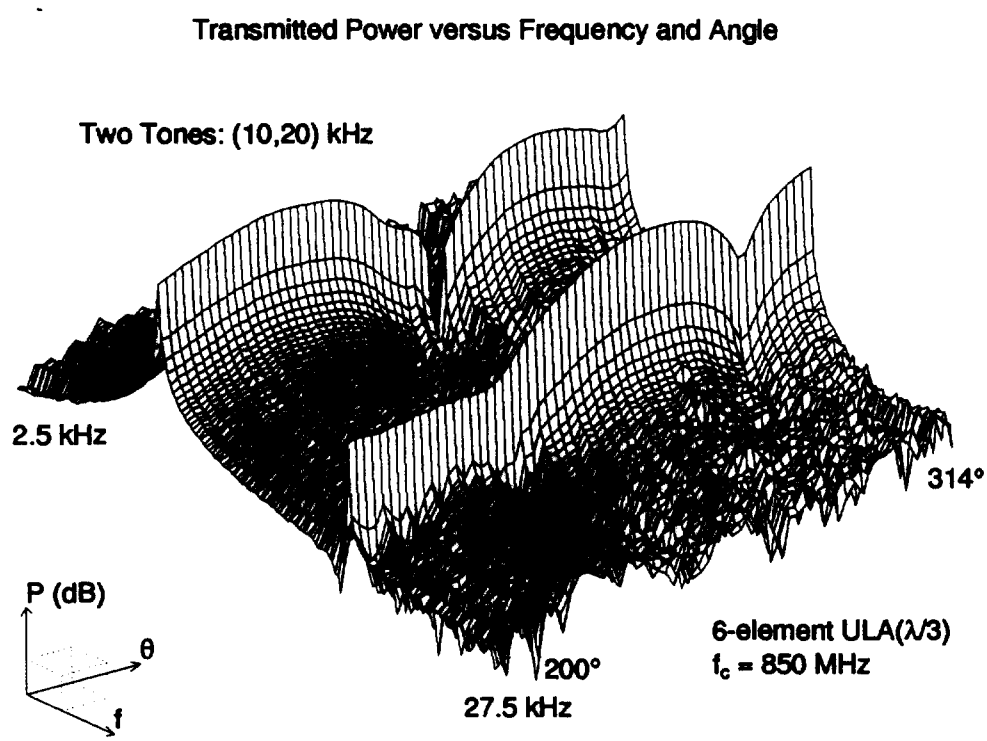

Figure 4-10: Measured spatial and frequency directivity for 10KHz and 20KHz tones directed to 225° and 270° respectively

4.2.2 BPSK signals

In this set of tests, the two BPSK waveforms described earlier were transmitted with the same objectives as applied to the dual sine wave tests. The feasibility of the SDMA transmission scheme was demonstrated by demodulating the waveforms received at various azimuths and performing direct comparisons with the transmitted bit streams. The results of these tests are shown in Figures 4-11 through 4-13. In Figure 4-11, successful demodulation (*i.e.* with no bit errors) of the signal directed to 270° is manifest over a minimum of a 12° sector about the intended transmission azimuth. The effects of a decreasing C/I ratio are evident at azimuth 274°.

In Figure 4-12, successful demodulation of the signal directed to 225° is obtained over a 6° sector about the intended transmission azimuth. Consistent with the previous observations concerning the breadth of the null achievable at 225°, there is no discernible performance degradation over the azimuth interval. Further evidence of the breadth of the null is given in Figure 4-13 wherein successful demodulation is shown out to 240°. As in the tone tests, SDMA succeeds in directively transmitting information while simultaneously minimizing total transmitted power.

At azimuths far from the selected transmission azimuths, we note that successful demodulation may not be achievable. This effect is illustrated by the results at 250° and 300°. Significantly less power is transmitted in those directions, resulting in increased estimate variances.

4.3 Office Environment Experiments: FM Transmission

In the office building interior tests, the signal sources were provided by recorded music played back on standard cassette players. These sources were sampled at a 50KHz rate, digitally FM modulated at baseband, spatially multiplexed and then upconverted to 850MHz by the transmitters. The receiver was a commercially available FM radio scanner and was tuned to the nominal 850MHz carrier.

In a typical test, transmission azimuths of, say, 90° (broadside) and 50° would be selected and an appropriate spatial multiplexing strategy computed. A separate music signal would be transmitted in each direction and the experimenter would listen to the received signal as the receiver was moved about the building interior. Transmitter to receiver distances in the experiments were as large as 20m (transmitted power was deliberately held below 0dBm as these were "on-air" tests outside of a shielded environment). In these tests, too, SDMA successfully directed each signal to its desired azimuth while simultaneously suppressing interference from the other signal. The very successful results of this test were, to be frank, a pleasant surprise in light of the rudimentary nature of the experimental apparatus. The inside of an office building presents a stressful RF environment due to intervening walls, structural steel, electrical conduits, etc. These results of these tests provide validation for SDMA in a realistic communications environment.

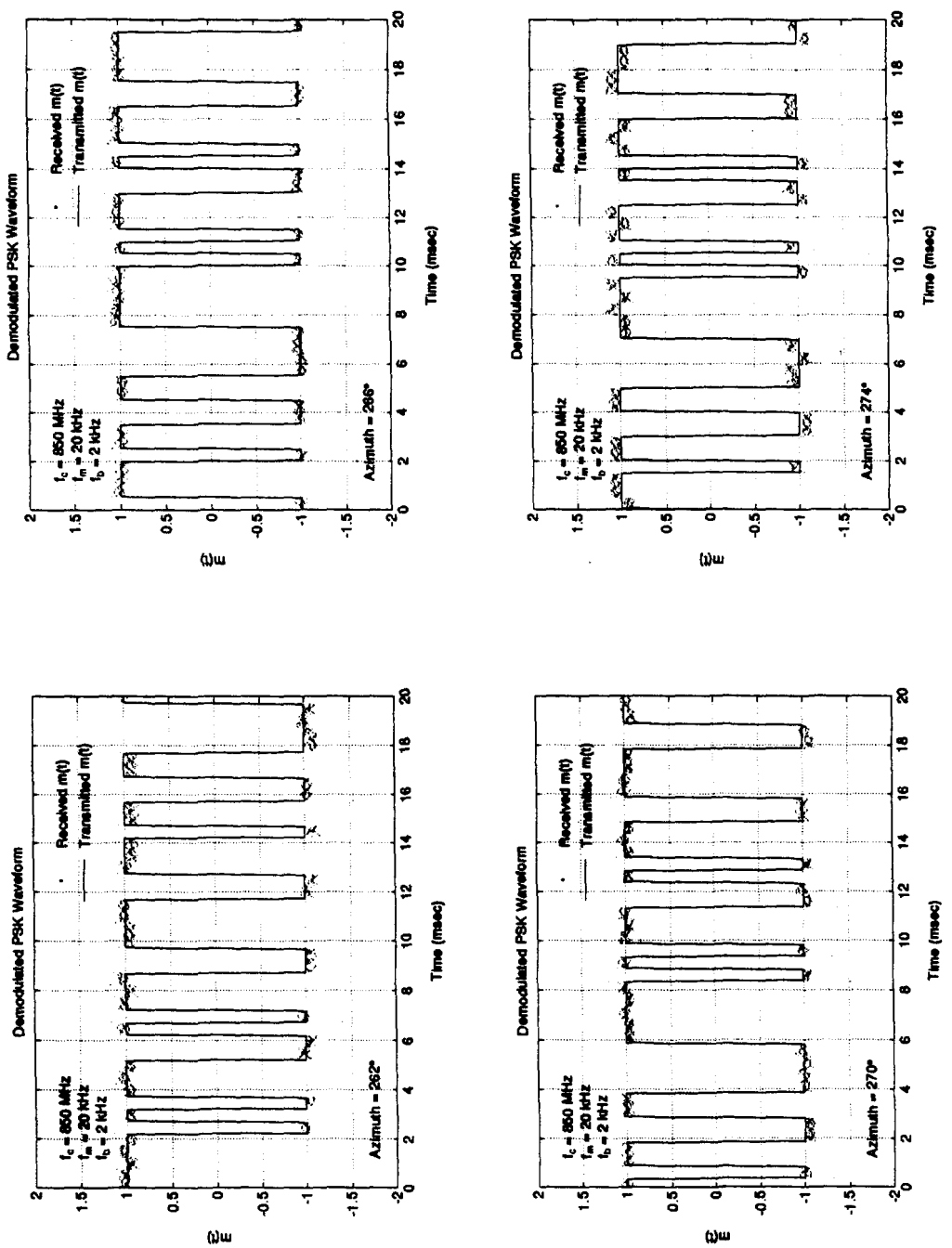

Figure 4-11: BPSK transmitted and received bit sequences around 270°

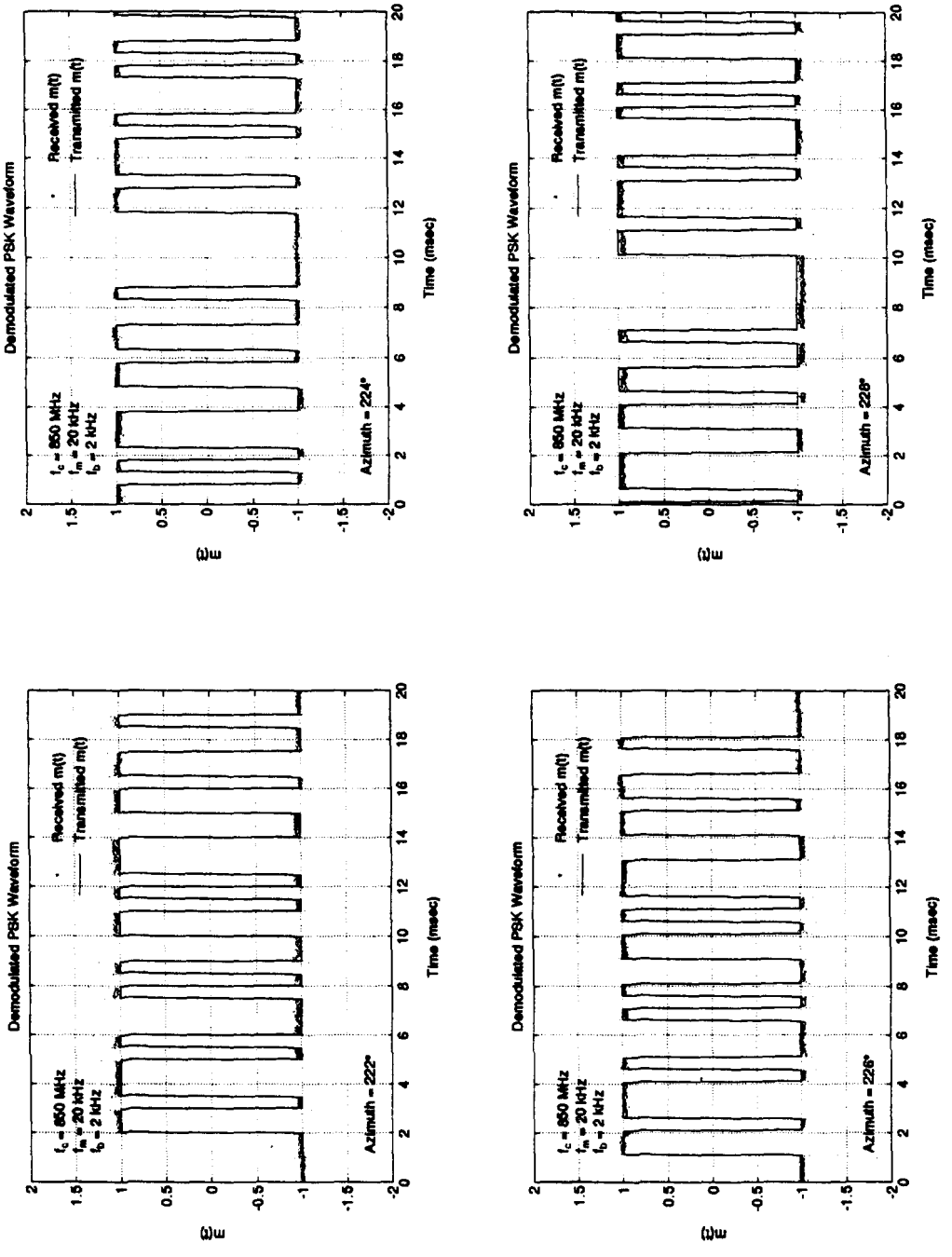

Figure 4-12: BPSK transmitted and received bit sequences around 225°

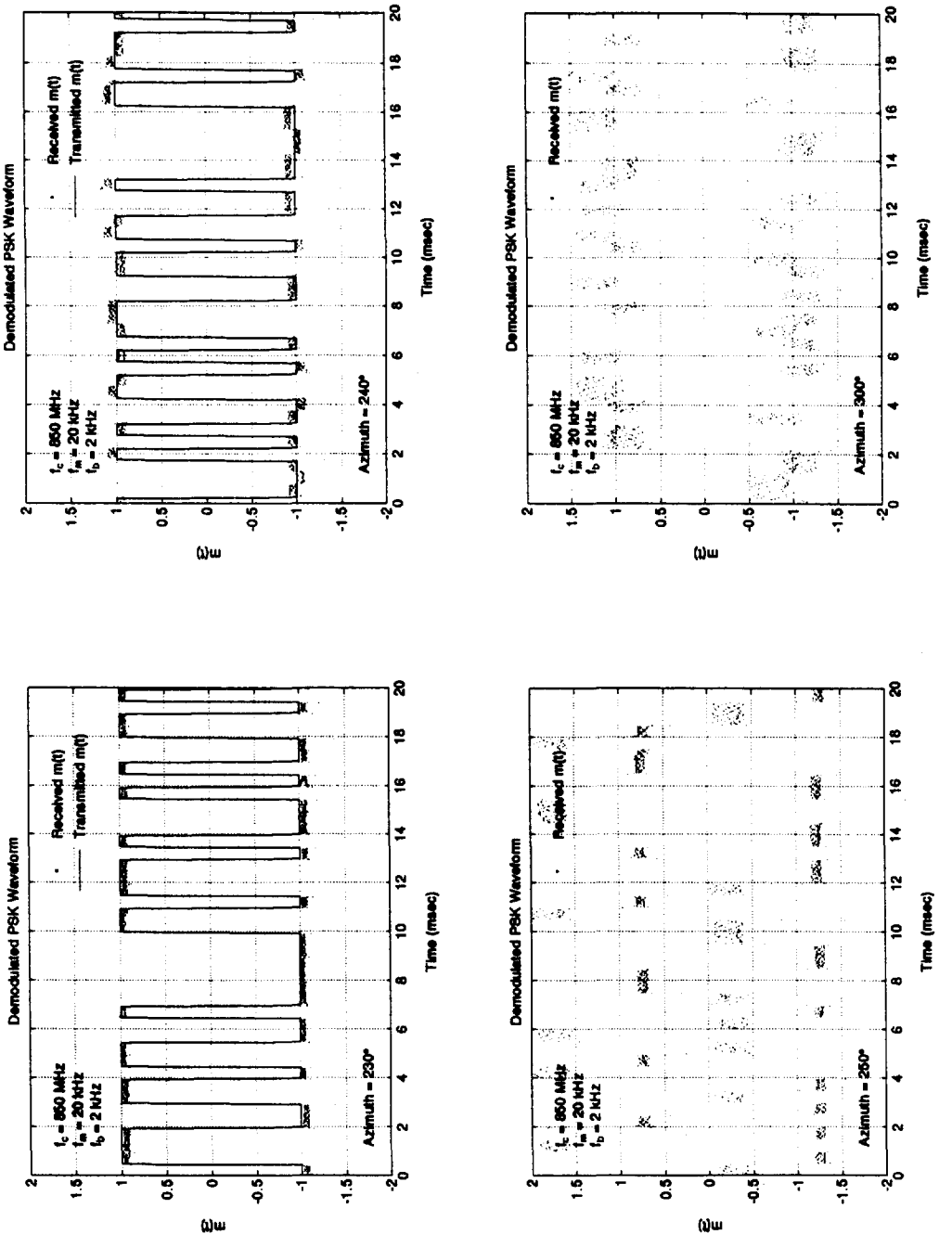

Figure 4-13: Received/Demodulated message sequences at various azimuths

5. Conclusions

Prototype systems were constructed to demonstrate SDMA's ability to spatially transmit and receive multiple signals on a single frequency channel. Two sets of experiments were conducted. The first set took place in an anechoic chamber to assess SDMA's performance in a "clean" RF environment with both pure tone signals and digital communications signals. The second set of experiments was conducted in an office building interior to provide a RF environment typical of that for, say, a PCS system. Frequency modulated music signals were employed for these latter tests. In all reception tests, the spatial locations of the transmitters were correctly estimated and the transmitted signals correctly demodulated. SDMA's capability to establish distinct spatial transmission channels was also clearly demonstrated by these tests. The tests conducted in the office building interior are especially significant, as they validate the technology in an environment that is representative of a typical commercial application. We note that the prototype system was constructed of commercially available, off-the-shelf, components and at a modest cost.

The potential impact of SDMA in WCN applications — increased capacity, increased service availability, and increased service quality, all at a modest incremental base station cost and compatible with existing customer equipment — clearly make this technology worthy of additional funding for development. The Phase II effort will be to build an operational full-duplex prototype that would demonstrate the ability to simultaneously locate, track, and communicate with multiple mobile wireless units from a single base station. This apparatus will be instrumental in performing investigations of the applicability of the technology in RF environments of varying degrees of complexity. It will provide a key research tool for the identification of SDMA system issues requiring further investigation and for evaluating candidate solutions thereto, taking the SDMA concept another step closer to reality.

A. Algorithmic Details

The purpose of this appendix is to briefly describe the algorithmic underpinnings of SDMA. An extensive technical literature concerning direction of arrival (DOA) estimation exists, we refer the reader to the bibliography contained in the Phase I proposal for a starting point. Here, the emphasis is on the ***ESPRIT*** (Estimation of Signal Parameters via Rotational Invariance Techniques) algorithm whose accuracy and computational simplicity make it particularly well suited to SDMA.

The Narrowband Data Model

Though ***ESPRIT*** is generally applicable to a wide variety of problems, for obvious reasons the discussions herein focus on DOA estimation. Data from an array of sensors are collected and the objective is to locate point sources assumed to be radiating energy that is detectable by the sensors. Herein, the transmission medium is assumed to be isotropic and non-dispersive so that the radiation propagates in *straight lines*, and the sources are assumed to be in the *far-field* of the array. For the ranges of RF's considered herein, this assumption is easily shown to valid. Consequently, the radiation impinging on the array is in the form of a sum of *plane waves*. For simplicity, it will initially be assumed that the problem is planar, thus reducing the location parameter space to a single-dimensional subset of $\Re$, *i.e.*, $\theta_i \in [-\pi, \pi]$, where θ_i is the direction-of-arrival (DOA) of the i^{th} source. Assuming the signals are *narrowband* and have the same *known* center frequency, ω_0, $x_k(t)$, the complex signal output of the k^{th} sensor at time t, can be written as

$$x_k(t) = \sum_{i=1}^{d} a_k(\theta_i) s_i(t - \tau_{ki}) = \sum_{i=1}^{d} a_k(\theta_i) s_i(t) e^{-j\omega_0 \tau_{ki}} , \tag{A.1}$$

where τ_{ki} is the propagation delay between a reference point and the k^{th} sensor for the i^{th} wavefront impinging on the array from direction θ_i, $a_k(\theta_i)$ is the corresponding sensor element complex response (gain and phase) at frequency ω_0, and there are assumed to be d point sources present.

Employing vector notation for the outputs of the m sensors, the *data model* becomes

$$\mathbf{x}(t) = \sum_{i=1}^{d} \mathbf{a}(\theta_i) s_i(t) , \tag{A.2}$$

where $\mathbf{a}(\theta_i) = [a_1(\theta_i)e^{-j\omega_0\tau_1(\theta_i)}, \ldots, a_m(\theta_i)e^{-j\omega_0\tau_m(\theta_i)}]^T$, often termed the *array steering vector* for direction θ_i. Setting $\mathbf{A}(\boldsymbol{\theta}) = [\mathbf{a}(\theta_1), \ldots, \mathbf{a}(\theta_d)]$, $\mathbf{s}(t) = [d_1(t), \ldots, d_d(t)]^T$, and adding measurement noise $\mathbf{n}(t)$, the *measurement model* for the passive sensor array narrowband signal processing problem is

$$\mathbf{z}(t) = \mathbf{A}(\boldsymbol{\theta})\mathbf{s}(t) + \mathbf{n}(t) . \tag{A.3}$$

Note that $\mathbf{z}(t), \mathbf{n}(t) \in \mathbb{C}^m$, $\mathbf{s}(t) \in \mathbb{C}^d$, and $\mathbf{A}(\boldsymbol{\theta}) \in \mathbb{C}^{m \times d}$, and it is assumed that $m > d$.

ESPRIT enjoys a significant reduction in computational complexity relative to most DOA algorithms, obtained by imposing a simple constraint on the structure of the sensor array. The constraint is most easily described by an example. Consider a planar array of arbitrary geometry composed of $M/2$ sensor *doublets* as shown in Figure A-1. The

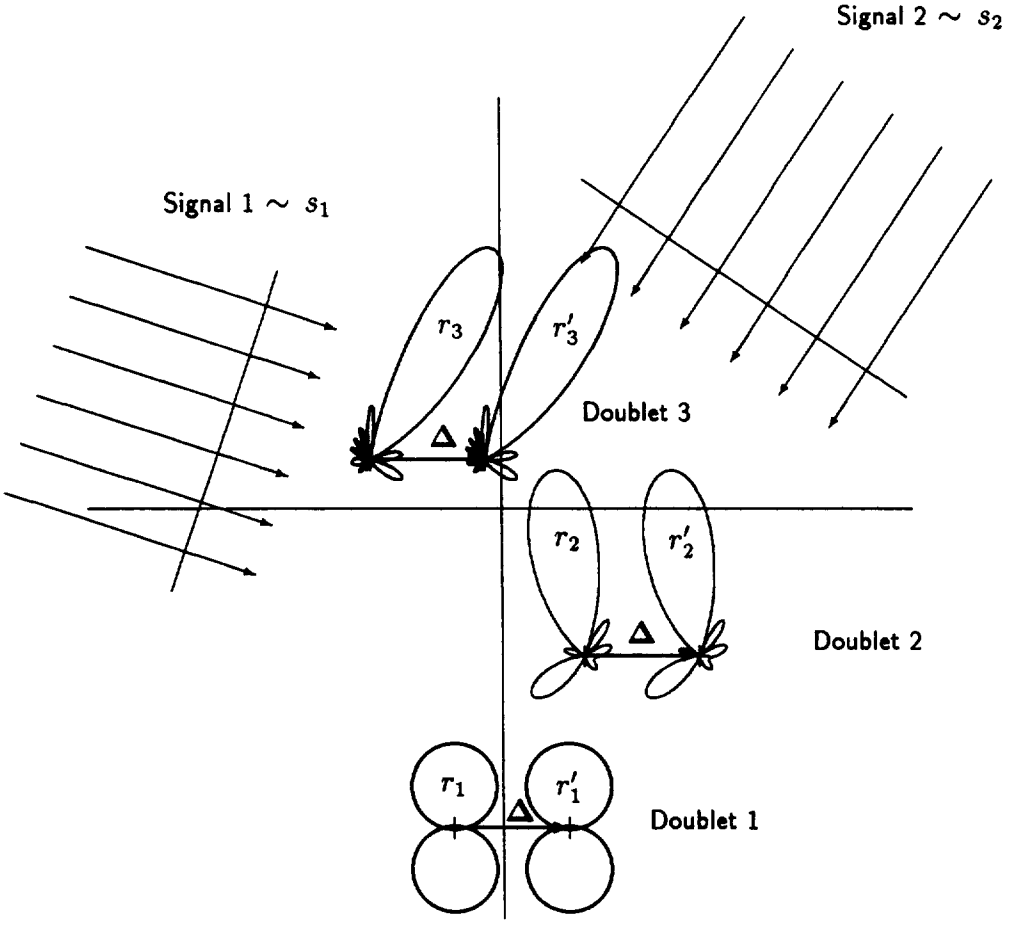

Figure A-1: Sensor Array Geometry for Multiple Source DOA Estimation Using ***ESPRIT***

elements in each doublet have identical sensitivity patterns and are translationally separated by a known constant displacement vector $\boldsymbol{\Delta}$. Other than the obvious requirement that each sensor have non-zero sensitivity in all directions of interest, the gain, phase, and polarization sensitivity of the elements in the doublet are arbitrary. Furthermore, there is no requirement that any of the doublets possess the same sensitivity patterns, though as discussed in [1], there are advantages to employing arrays with such characteristics such as uniform linear arrays (ULA's).

ESPRIT Data Model

Assume that there are $d \leq m$ (m is the number of sensors in each subarray) narrowband sources[1] centered at frequency ω_0, and that the sources are located sufficiently far from the array such that in homogeneous isotropic transmission media, the wavefronts impinging on the array are planar. As before, the sources may be assumed to be stationary zero-mean random processes or deterministic signals. Additive noise is present at all $M = 2m$ sensors and as before is assumed to be a stationary zero-mean random process with a *spatial* covariance $\sigma^2\mathbf{I}$. There is no loss of generality in comparison with the assumption that the covariance is $\sigma^2\mathbf{\Sigma}_n$. As long as $\mathbf{\Sigma}_n$ is known, *pre-whitening* of the measurement noise can be performed, or generalized singular value or eigendecompositions can be employed.

To describe mathematically the effect of the *translational invariance* of the sensor array, it is convenient to describe the array as being comprised of two subarrays, Z_0 and Z_1, identical in every respect although physically displaced (not rotated) from each other by a known displacement vector $\mathbf{\Delta}$. The signals received at the i^{th} doublet can then be expressed as

$$\begin{aligned} z_i^{(0)}(t) &= \sum_{k=1}^{d} s_k(t)a_i(\theta_k) + n_{0i}(t), \\ z_i^{(1)}(t) &= \sum_{k=1}^{d} s_k(t)e^{j\omega_0 \Delta \sin\theta_k/c}a_i(\theta_k) + n_{1i}(t), \end{aligned} \tag{A.4}$$

where θ_k is the direction of arrival of the k^{th} source relative to the direction of the translational displacement vector $\mathbf{\Delta}$.

Combining the outputs of each of the sensors in the two subarrays, the received data vectors can be written as follows:

$$\mathbf{z}_0(t) = \mathbf{A}_0\mathbf{s}(t) + \mathbf{n}_0(t)\,, \tag{A.5}$$

$$\mathbf{z}_1(t) = \mathbf{A}_0\mathbf{\Phi}\mathbf{s}(t) + \mathbf{n}_1(t)\,, \tag{A.6}$$

where the vector $\mathbf{s}(t)$ is the $d \times 1$ vector of impinging signals (wavefronts) as observed at the reference sensor of subarray Z_0, and $\mathbf{A}_0$ is the array response vector associated with Z_0. The individual signals can be temporally correlated, *i.e.*, $E\{s_i(t)s_j^*(t)\} \neq 0$, $i \neq j$. Coherent (or fully correlated) sources can easily be handled as discussed in the next section if there are multiple invariances in the array. However, coherent sources can not be uniquely located with only a single array invariance and unknown array manifold vectors. The matrix $\mathbf{\Phi}$ is a diagonal $d \times d$ matrix of the phase delays between the doublet sensors for the d wavefronts and may be written as $\mathbf{\Phi} = \mathrm{diag}[e^{j\gamma_1}, \ldots, e^{j\gamma_d}]$, where $\gamma_k = \omega_0\Delta\sin\theta_k/c$. $\mathbf{\Phi}$ is a unitarymatrix (operator) that relates the measurements from subarray Z_0 to those from subarray Z_1.

[1]**MUSIC** imposes the requirement $d < 2m$, and can therefore can handle roughly twice as many sources as ***ESPRIT*** in general. For uniform linear arrays, however, ***ESPRIT*** can handle as many sources as **MUSIC** by employing *overlapping* subarrays.

Defining the total array output vector as $\mathbf{z}(t)$, the subarray outputs can be combined to yield

$$\mathbf{z}(t) = \begin{bmatrix} \mathbf{z}_0(t) \\ \mathbf{z}_1(t) \end{bmatrix} = \bar{\mathbf{A}}\mathbf{s}(t) + \mathbf{n}_z(t), \tag{A.7}$$

where

$$\bar{\mathbf{A}} = \begin{bmatrix} \mathbf{A}_0 \\ \mathbf{A}_0\mathbf{\Phi} \end{bmatrix}, \quad \mathbf{n}_z(t) = \begin{bmatrix} \mathbf{n}_0(t) \\ \mathbf{n}_1(t) \end{bmatrix}. \tag{A.8}$$

$$\tag{A.9}$$

It is the structure of $\bar{\mathbf{A}}$ that is exploited to obtain estimates of the diagonal elements of $\mathbf{\Phi}$ *without prior knowledge of* $\mathbf{A}_0$.

In its single invariance, eigenvalue decomposition version, the ***ESPRIT*** algorithm operates as follows. Details can be found in [1, 2].

1. Obtain an estimate of $\mathbf{R}_{zz}$, denoted $\widehat{\mathbf{R}}_{zz}$, from the measurements.

2. Compute the eigen-decomposition of $\widehat{\mathbf{R}}_{zz}$

$$\widehat{\mathbf{R}}_{zz}\bar{\mathbf{E}} = \bar{\mathbf{E}}\mathbf{\Lambda},$$

   where $\mathbf{\Lambda} = \text{diag}\{\lambda_1, \ldots, \lambda_M\}$, $\lambda_1 \geq \cdots \geq \lambda_M$, and $\bar{\mathbf{E}} = [\mathbf{e}_1 \,\vdots\, \cdots \,\vdots\, \mathbf{e}_M]$.

3. Estimate the number of sources $\hat{d}$ using the minimum description length statistical criterion.

4. Obtain the signal subspace estimate $\hat{\mathcal{S}}_z = \mathcal{R}\{\hat{\mathbf{E}}_s\} \stackrel{\text{def}}{=} [\mathbf{e}_1 \,\vdots\, \cdots \,\vdots\, \mathbf{e}_{\hat{d}}]$ and decompose it using a *selection matrix* $\mathbf{J}$ according to a particular choice of subarrays,

$$\mathbf{J}\hat{\mathbf{E}}_s = \begin{bmatrix} \hat{\mathbf{E}}_0 \\ \hat{\mathbf{E}}_1 \end{bmatrix}.$$

5. Compute the eigendecomposition $(\lambda_1 > \ldots > \lambda_{2\hat{d}})$,

$$\hat{\mathbf{E}}_{01}^*\hat{\mathbf{E}}_{01} \stackrel{\text{def}}{=} \begin{bmatrix} \hat{\mathbf{E}}_0^* \\ \hat{\mathbf{E}}_1^* \end{bmatrix} [\hat{\mathbf{E}}_0 \,\vdots\, \hat{\mathbf{E}}_1] = \mathbf{V}\mathbf{\Lambda}\mathbf{V}^*,$$

   and partition $\mathbf{V}$ into $\hat{d} \times \hat{d}$ submatrices,

$$\mathbf{V} \stackrel{\text{def}}{=} \begin{bmatrix} \mathbf{V}_{11} & \mathbf{V}_{12} \\ \mathbf{V}_{21} & \mathbf{V}_{22} \end{bmatrix}.$$